Mitigation of tip vortex cavitation by means of air injection on a Kaplan turbine scale model

A Rivetti[1], M Angulo[1], C Lucino[1], S Liscia[1]

Laboratory of Hydromechanics, Faculty of Engineering, National University of La Plata, 47 Nº 200, La Plata, Argentina.

E-mail: arturorivetti@gmail.com.

Abstract. Kaplan turbines operating at full-load conditions may undergo excessive vibration, noise and cavitation. In such cases, damage by erosion associated to tip vortex cavitation can be observed at the discharge ring. This phenomenon involves design features such as (1) overhang of guide vanes; (2) blade profile; (3) gap increasing size with blade opening; (4) suction head; (5) operation point; and (6) discharge ring stiffness, among others. Tip vortex cavitation may cause erosion at the discharge ring and draft tube inlet following a wavy pattern, in which the number of vanes can be clearly identified.
Injection of pressurized air above the runner blade centerline was tested as a mean to mitigate discharge ring cavitation damage on a scale model. Air entrance was observed by means of a high-speed camera in order to track the air trajectory toward its mergence with the tip vortex cavitation core. Post-processing of acceleration signals shows that the level of vibration and the RSI frequency amplitude decrease proportionally with air flow rate injected. These findings reveal the potential mitigating effect of air injection in preventing cavitation damage and will be useful in further tests to be performed on prototype, aiming at determining the optimum air flow rate, size and distribution of the injectors.

1. Introduction

Depending on operating conditions and main design features, cavitation in Kaplan turbines may develop at different locations, mostly on both sides and tip of the blades, hub and discharge ring, following different patterns of structure, extension and dynamic behavior [1]. Cavitation induces vibration and noise emission. Investigation on physical models has demonstrated that the levels of vibration and noise emission are correlated to the decrease of the Thoma cavitation number (σ) and that their corresponding signals are modulated by the frequency of blade passage [2].

Of all the mechanisms that promote erosive cavitation, the tip gap vortex cavitation caused by tip clearance flow is of particular interest because of its potential aggressiveness towards both the blade suction side, the discharge ring and draft tube inlet surface. In connection with the development of tip vortex cavitation, Kaplan turbines may experience, when operating at full-load condition, excessive cavitation along with severe vibration and noise emission.

Under such conditions, the outflow of the guide vanes and its pressure field are not uniform along the circumference. This may interfere with the non-stationary pressure field derived by the passage of the runner blades, thus giving rise to the so-called rotor stator interaction (RSI) [3]. This phenomenon, often seen in Francis and pump-turbines, might also appear in Kaplan turbines when guide vane overhang is likely to occur, as discussed in previous works [4, 5]. RSI in Kaplan turbines is a plausible

explanation for the specific pattern of cavitation frosting usually found on the discharge ring, occurring only at distinct locations corresponding to the number of guide vanes, as discussed by Nennemann [6] on the basis of computational fluid dynamics (CFD) simulations.

Injection of pressurized air has been proposed as a remediating procedure aimed at mitigating the effects of cavitation erosion and vibration at stationary components at the expense of a mild drop of the hydraulic efficiency of the turbine. Care should be taken in the determination of the most appropriate air injection rate as, if too high, such drops might become unacceptable.

In this paper, model tests with air injection above the runner blade centerline are presented. Acceleration signals were post-processed in order to analyze the potential mitigating effect of air injection of cavitation damage and severe vibration.

The study introduced herein was carried out under the framework of a project focused on the dynamic behavior of Kaplan turbines that combines prototype measurements, model tests and CFD simulations, and is supported by the Yacyretá Binational Entity (EBY), the National University of La Plata, Argentina (UNLP) and the National University of Misiones, Argentina (UNAM).

2. Methods and Materials

2.1. Test rig model scale

Experiments were performed at the Laboratory of Hydromechanics of the National University of La Plata, Argentina. The test rig is a closed circuit that allows for the testing of Kaplan and Francis turbines (Fig. 1). The model test was carried out in compliance with the IEC 60193 standard [7]. The error made in the calculation of efficiency is less than 0.24 %.

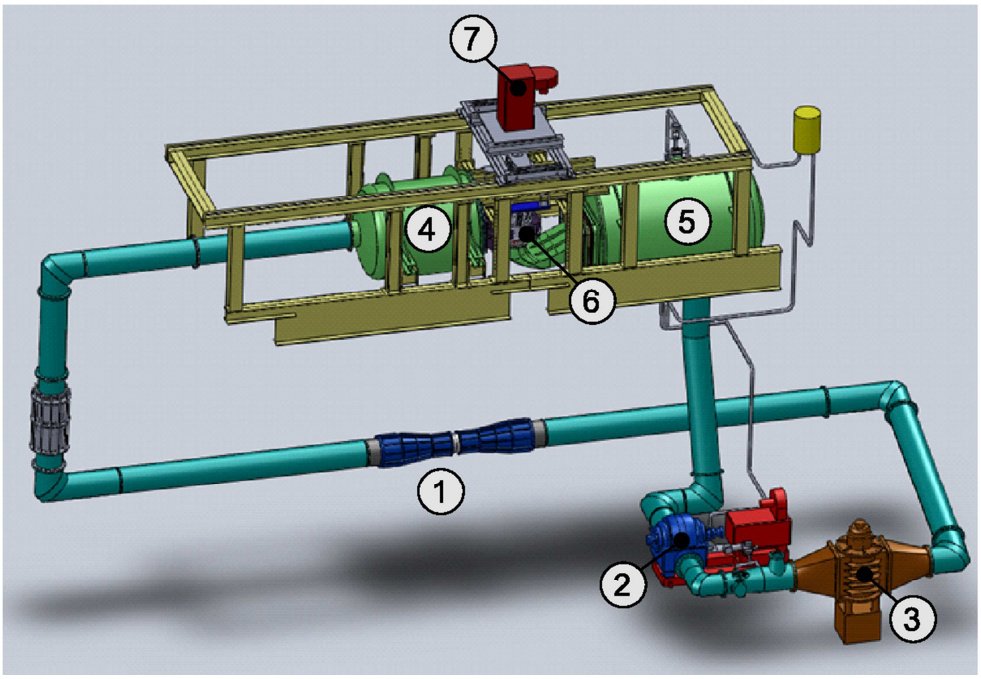

Figure 1. Test rig facility at the Laboratory of Hydromechanics of La Plata, Argentina. (1) Venturi flowmeter; (2) Recirculation pump; (3) Dissipation valve; (4) High-pressure tank; (5) Low-pressure tank; (6) Kaplan turbine; (7) Generator.

The scale model was a five-blade Kaplan turbine with twenty-four stay and guide vanes. Its diameter was D = 340 mm and its specific speed was ns = 614. The rotational speed during the test was n = 1000 rpm, which yields a Reynolds number of Re = 6.05×10^6, based on the blade tip velocity. The model was placed in the test rig between the high- and low-pressure tanks. The head was adjusted by varying the rotational speed of the recirculation pump. The low-pressure tank is equipped with a vacuum pump and a pneumatic controlled valve allowing for the variation of the absolute pressure of the system, in order to set the desired Thoma cavitation number (σ). Indeed, σ is given by Eq. 1:

$$\sigma = \frac{\left(\frac{p_b - p_v}{\gamma}\right) + hs}{H} \qquad \text{(Eq. 1)}$$

Where p_b = pressure at low-pressure tank, p_v = vapor pressure, γ =water specific weight, h_s = suction head, H = net head. Given that the test was carried out at constant head, flow rate and rotational speed, it becomes apparent from Eq. 2 that σ can be modified only by varying the pressure at the low pressure tank.

2.2. Air injection

Air was injected on the horizontal plane of the discharge ring. This location is in correspondence with the aeration conduct that is present in the prototype machine. Twenty evenly spaced holes of 3 mm diameter were connected to a 100 mm-diameter stainless-steel manifold through tubes. The volume of the manifold, allowing for a constant air injection pressure, along with the fact that all tubes are of the same length, both ensure that the discharge coefficient is the same at every injection point. Two air flowmeters (with different ranges) were placed between the manifold and the air compressor (Table 1). An arrangement of on/off valves allows for the use of the more appropriate one, depending on the amount of air injected. The air flow rate, Q_a, is adjusted with a needle valve (Fig. 2a).

Table 1. Air flow meters.

Brand	Model	Type	Range lps*	Accuracy %	Repeatability %
Hedland	H271B	Spring-Piston	0.40-2.60	2.0	1.0
Odin	RCP	Ball air flow meter	0.03-0.43	5.0	2.0

*STP, estándar condition for temperature and pressure (20°C, 1 atm)

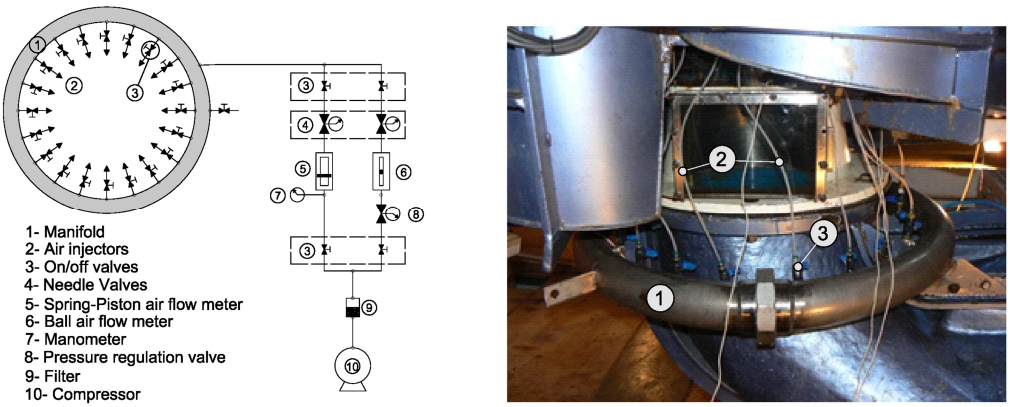

Figure 2. (a) Air injection system layout (b) Picture of air injection system mounted on the Kaplan model.

2.3 Monitoring system

Acceleration measurements: Three Endevco Isotron 2256A-100 accelerometers, with a flat frequency response from 0.1 Hz to 20 kHz, were placed at the discharge ring (Fig. 3b). The typical mounted resonance frequency is 25 kHz. The accelerometers were connected to an amplifier Endevco and the acquisition frequency was 20 kHz. The AC1 is located just below the injection plane; the AC2, on the blade passage plane; and the AC3, at the draft tube inlet.

High-speed flow visualization and lighting setup: The air injection and its influence on the development of cavitation were visualized by means of a high-speed velocity camera Photron FASTCAM SA4 with a CMOS color sensor connected to an acquisition computer. A resolution of 1024x860 at 3600 fps was chosen so as to obtain one frame every 1.66 degrees of runner rotation. Three 1000-watt sources equipped with linear tungsten halogen bulb type were used for lighting (Fig. 3c).

Data acquisition: Acceleration signals were simultaneously sampled with a 16-bit resolution at a 20 kHz sampling rate during 40 seconds for every measured point. Data sampling and post-processing were performed with software developed in LABVIEW.

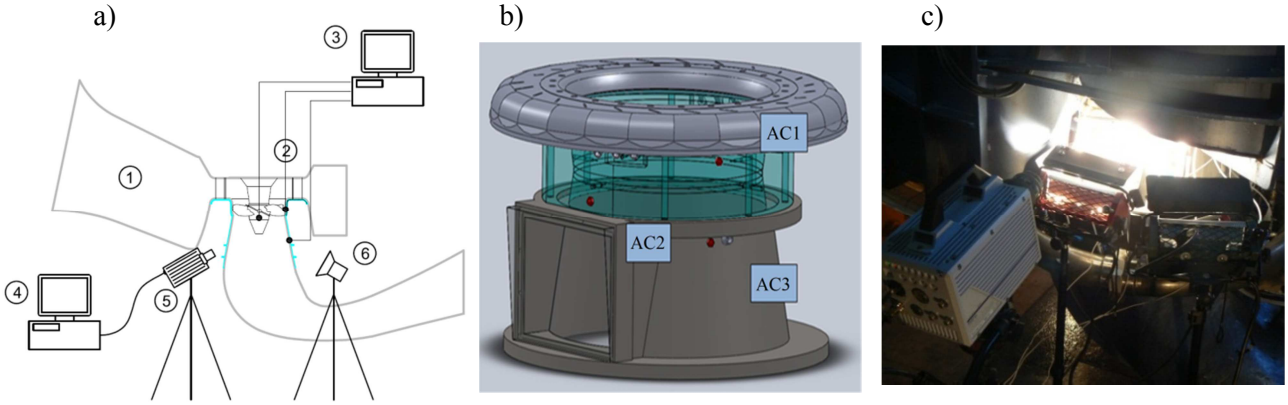

Figure 3. (a) Experimental setup: 1) Kaplan model; 2) Instrumentation; 3) Data acquisition system; 4) Video recorder computer; 5) High-speed camera; 6) Tungsten halogen lamps; (b) Accelerometers location; (c) High-speed camera and lighting arrangement on the model scale.

2.5. Operational condition and test proceeding

An operational point of high discharge for the normal operation head corresponding to the prototype machine was chosen for the experiment. This point corresponds to an ON CAM combination.

For this condition, the speed factor was $n_{ED} = 0.55$ and the discharge factor $Q_{ED} = 0.61$. Only the cavitation number was modified by adjusting the absolute pressure in the low-pressure tank covering a range going from $\sigma = 2.26$ (no cavitation) to $\sigma = 0.66$ (full cavitation).

A series of tests were performed wherein the cavitation number was swept over the range 0.660–2.260 in a stepwise manner, whereas the amount of air injected was likewise increased for $\sigma^* = 0.946$. The upper limit corresponds to a cavitation-free operating condition. The cavitation number is decreased by gradually diminishing the pressure of the test rig circuit. A total of ten steps were considered until cavitation was fully developed. The maximum air flow rate injected was 2 ‰ expressed as a fraction of the water flow rate, Q.

For every step the acceleration signal and the test rig state variables were acquired during 40 seconds. A video was recorded with the high-speed camera at 3600 fps for one second in order to study the air trajectory.

2.6. Data processing

Standard deviation of acceleration: The magnitude of the standard deviation st (Eq. 2) represents the level of vibration of the structural components of the model that is the response of the hydraulic forces, cavitation and vibration due to rotating components. It was calculated for every step registered.

$$st = \sqrt{\frac{1}{N}\sum_{i=1}^{N}(x_i - \bar{x})^2} \qquad \text{(Eq. 2)}$$

Where N = number of samples, i = dummy index, x_i = observed values, $\bar{x}$ = mean value.

Fast Fourier Transform: Standard FFT was done to study the acceleration signal in the frequency domain.

Demodulated analysis: The envelope of the signal was obtained using a Hilbert transform after applying a high pass filter at 60 *fn*. A FFT of this envelope was used to extract the frequency components and the amplitudes. The tip cavitation intensity and its interaction with the guide vanes could be identified with the frequency components corresponding to 5 *fn* (blade passage frequency) and 25 *fn* (RSI interaction) [3, 5]. Applying the same analysis for 20 injection points and five blades, a frequency of 20 *fn* was obtained. These components represent the interaction between the blade passage and the injection of air (RII, rotor injector interaction).

3. Results

3.1 High-speed flow visualization

3.1.1 Development of cavitation

It is apparent from Fig. 4 (where the development of cavitation as the cavitation number decreases is illustrated through a series of high-speed camera frames) that the flow through the runner is free of cavitation as long as σ does not fall below approximately 1.83. An incipient tip vortex can be observed for σ = 1.42, whose size increases as s decreases down to 0.66. Hub cavitation can also be seen for σ* = 0.946 and, for σ less than 0.77, a more generalized cavitation state, which includes trailing and leading edge cavitation and large bubbles at the discharge ring.

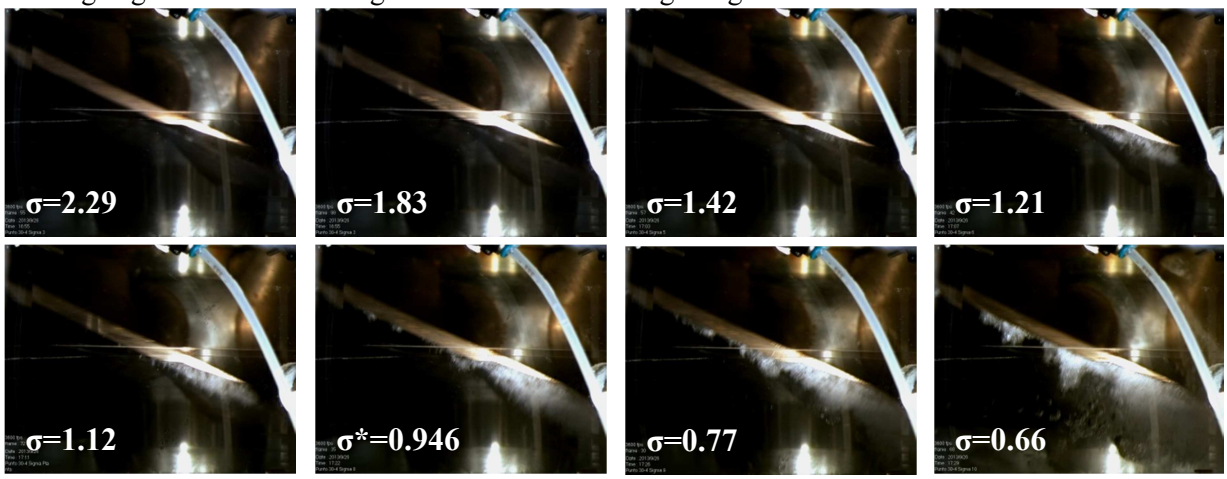

Figure 4. From left to right and top to bottom, video frame at same blade position for high to low cavitation number.

3.1.2 Air trajectory

Once injected, the air jet is seen to drift in the direction of the absolute velocity of water (frame 4) until being intersected by the passing blades (frame 7). The air thus absorbed by the blade tip suction side (red contour) slides on the blade contour until merging with the core of the tip vortex (frame 14), increasing the volume of the air bubbles.

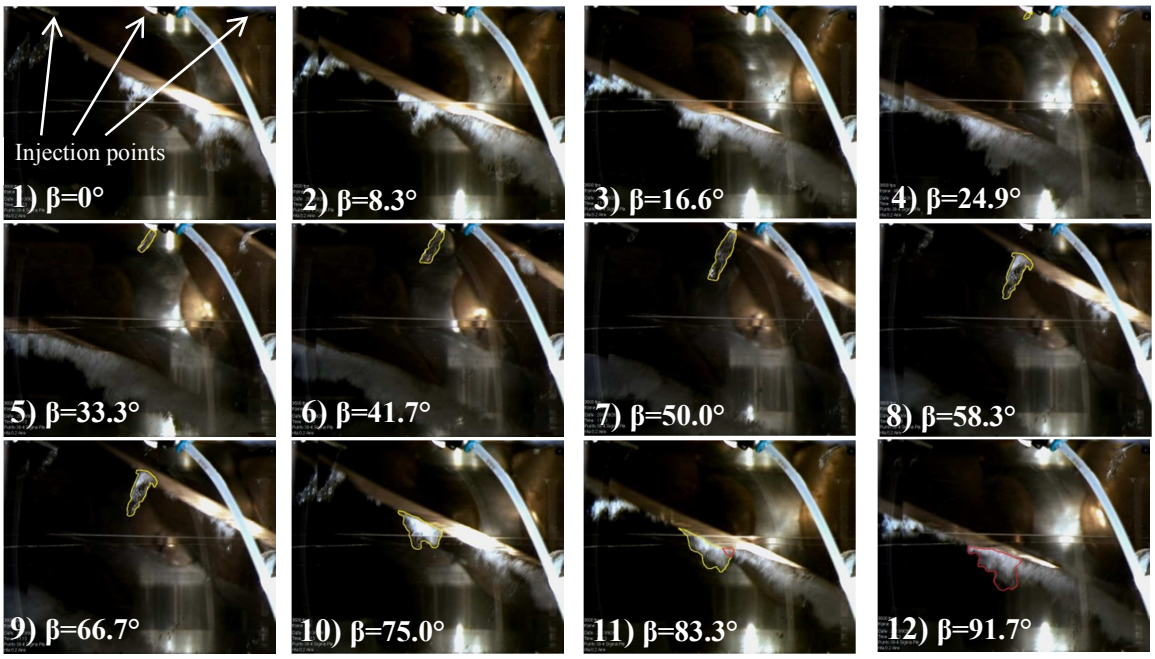

Figure 5. From left to right and from top to bottom, air injection and mixture with tip vortex cavitation under operating condition of constant head, constant flow rate and σ* = 0.946. Frames were taken every 8.3° of runner rotation, covering 1.3 times a blade passage. Air injected is denoted by yellow lines. Cavitation bubbles mixed with air are denoted by red lines.

3.2 Vibration

The level of vibration was quantified by the standard deviation of the acceleration signal (Fig. 6a). As the cavitation number was forced to decrease, a rise of the signal was observed until a local peak was reached for a value of σ between 0.9 and 1.2 (depending in which accelerometer is considered). This was followed by a drop that precedes a new, higher, peak related to fully developed cavitation. This kind of behavior had already been observed in a Kaplan scale model [2].

The injection of air was observed to attenuate the level of vibration, as seen in Fig. 6b, for σ* = 0.946. As can be seen, the minimum level of vibration was reached for an air injection rate of 0.8 ‰. Higher amounts of air did not induce any further reduction in the level of vibration.

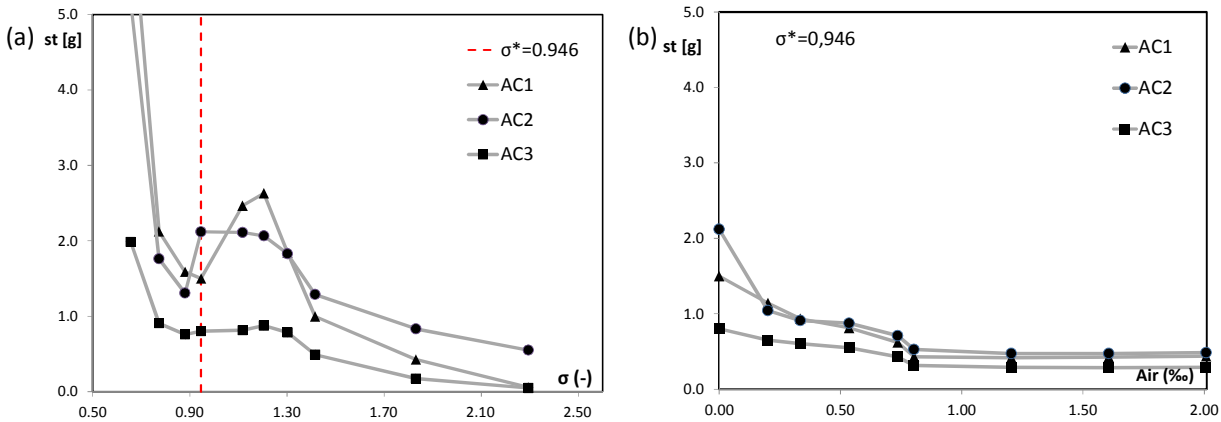

Figure 6. (a) Results of vibration levels at different cavitation numbers; (b) Vibration with air injection at constant σ. Air flow rate is expressed in terms of its ratio with respect to the model flow rate.

3.3 Frequency analysis

As can be deduced from the results of the fast Fourier transform of the acceleration signal (Fig. 5a), frequency components appear in a range from 5 to 50 *fn* under cavitation-free conditions (σ = 2.290). On the other hand, whenever σ* = 0.946, energy is spread in the range from 50 and 500 *fn*, with a peak at 200 *fn*. The two components visible at 25 *fn* and 50 *fn* are associated with rotor stator interaction (RSI). In the FFT of the envelope (Fig. 5b), the blade passage frequency (5 *fn*) and the RSI (25 *fn*) appear as the highest components.

The injection of 0.33 ‰ and 1.2 ‰ of air induces a displacement of the energy towards lower-frequency regions (10 to 100 *fn*). In the FFT of the signal and the envelope as well, the main component is 20 *fn* that is associated with the RII (rotor injector interaction).

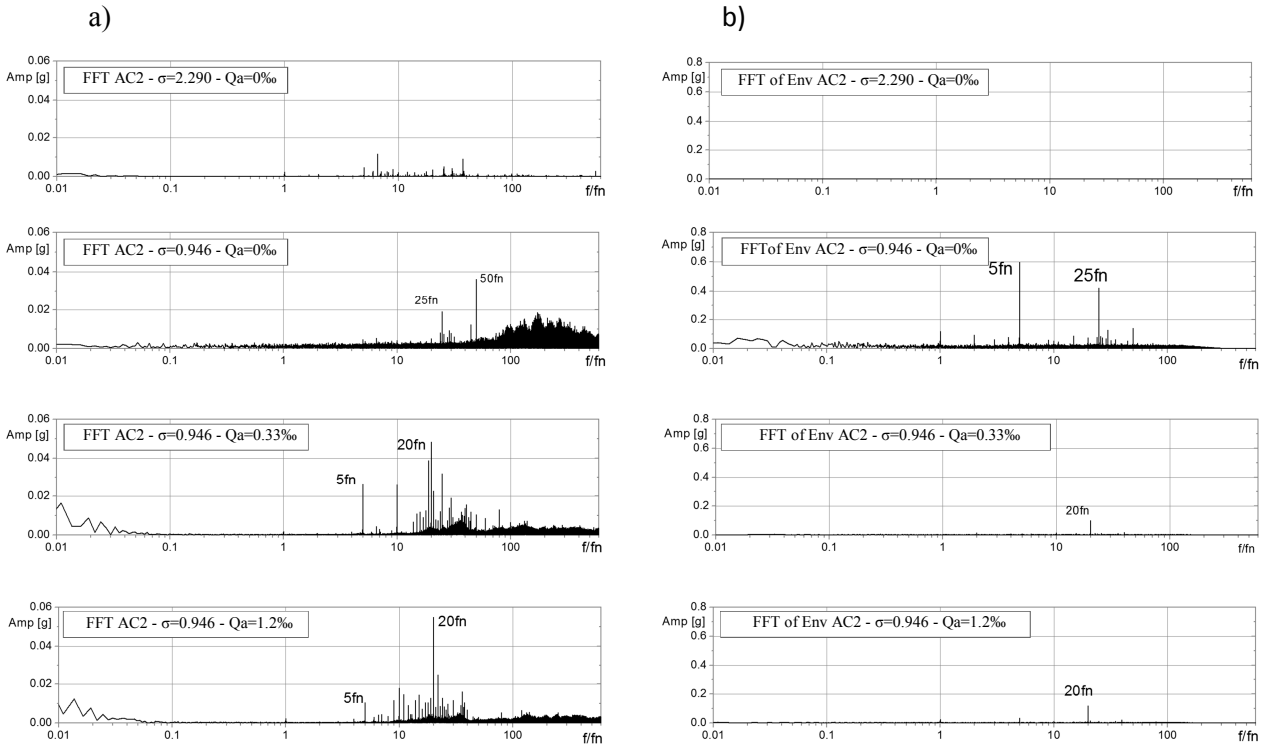

Figure 5. (a) FFT of accelerometer signal for high cavitation number, and study sigma with and without air injection; (b) FFT of the envelope of acceleration for the same condition shown in (a).

3.4 Efficiency

The effect of cavitation on the efficiency of the turbine is apparent from the mild decline for σ less than 1.42 (Fig. 8a), corresponding to the development of the tip vortex. Under operating conditions characterized by σ* = 0.946, such drop is as large as 1.7 %.

For all its advantages, air injection causes efficiency to drop with respect to air-free conditions (Fig. 8b). Such drop is less than 2 % for air flow rates up to 0.7 ‰, and less than 1 % for air flow rates less than 0.5 ‰. Greater air flow rates can affect efficiency dramatically, causing losses that can amount to up to 6.8 %.

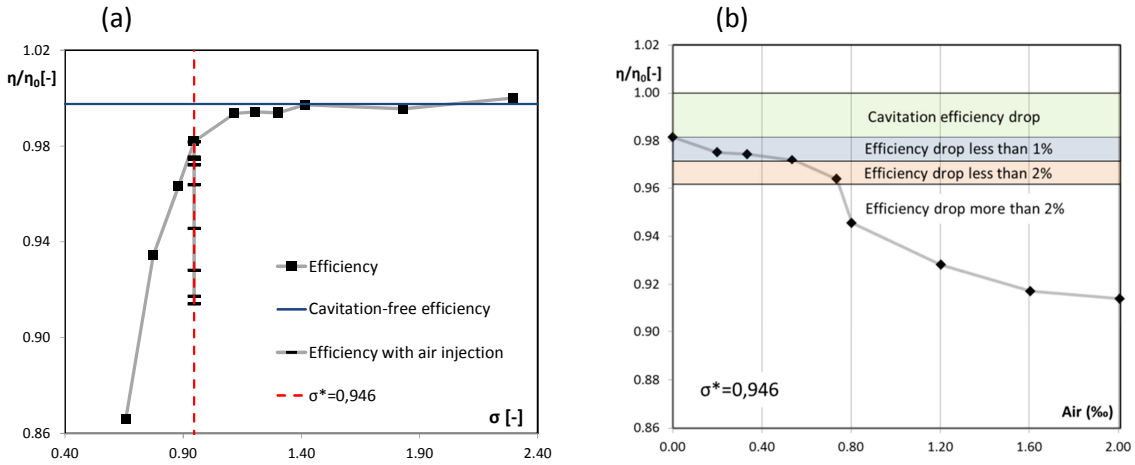

Figure 6. (a) Efficiency at different cavitation numbers. (b) Efficiency drop caused by air injection.

4. Discussion

4.1 Efficiency of air injection

The results presented in this work show the effectiveness of the air injection in the attenuation of the level of vibration due the tip vortex cavitation (Table 2). Vibration attenuation proved to be more pronounced for the AC2 since it is the nearest to the tip vortex cavitation development. For an amount of air injected of 0.33 ‰, the reduction of the level of vibration is 57 % for AC2, with an efficiency drop of 0.64 %.

Table 2. Vibration and efficiency drop at different air flow rates. The standard deviation *st* (columns 3 to 5) is referred to the vibration level without air injection s_0.

Step	Air flow rate	AC1	AC2	AC3	Efficiency drop
Nº	Qa [‰]	st/s_0 [-]	st/s_0 [-]	st/s_0 [-]	Δη [%]
1	0.00	1.00	1.00	1.00	0.00
2	0.20	0.76	0.49	0.81	0.64
3	0.33	0.62	0.43	0.75	0.71
4	0.54	0.54	0.41	0.68	0.96
5	0.74	0.41	0.33	0.54	1.78
6	0.80	0.29	0.25	0.39	3.61
7	1.20	0.28	0.22	0.36	5.36
8	1.61	0.28	0.22	0.36	6.45
9	2.01	0.29	0.23	0.36	6.77

4.2 Pressure fluctuation at injection points

A pressure diagram taken from a CFD simulation shows the pressure distribution along the horizontal plane on which injections points lie. It is apparent from the high-speed camera frames that the air entrance is not steady. This can be explained by the pressure distribution at the discharge ring. When the pressure of the flow is lower than the pressure at the manifold, air enters into the flow. When the pressure in the flow is higher, the air entrance stops until the pressure goes down again. This cycle

occurs at every injection point with the blade passage frequency, 5 *fn*. In the frequency analysis done in the previous section, the frequency component of 20 *fn* was found, suggesting the interaction with the blade passage and the 20 injections points.

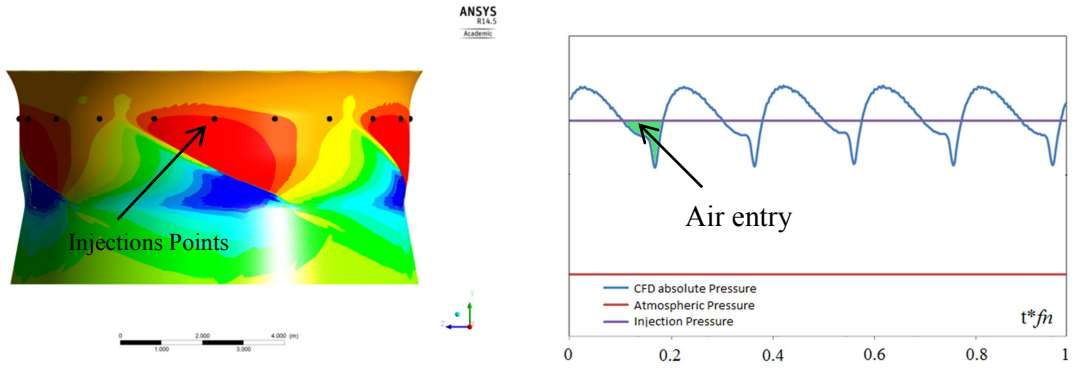

Figure 9. (a) CFD absolute pressure distribution at the discharge ring. Injection points are denoted by black dots; (b) Pressure fluctuation at one injection point for one runner revolution.

5. Conclusions

A series of cavitation tests were carried out on a scale model Kaplan turbine and air injection above the runner centerline was implemented with the aim of analyzing its influence on the mitigation of cavitation damage and levels of vibration.

Air injection was visualized by means of a high-speed camera so as to gain insight into the actual nature of the phenomenon, as the trajectory of air bubbles was described from the injection points to the core of the tip vortices. Air entrance was seen to take place with the pressure drop caused by the passage of blades. When the blade leading edge passes through an air injector, there is an impact with the air jet that occurs twenty times at every blade for a runner rotation. This effect is evidenced in the acceleration envelope where the frequency of 20 *fn* (RII) is dominant.

Vibration levels were correlated to the standard deviation of the signal of the acceleration, as measured at the discharge ring.

The tip vortex cavitation that develops at lower cavitation numbers was singled out as one of the main causes of the increase of vibration levels as the acceleration signal was observed to be modulated by the frequency of blade passage component (5 *fn* and 25 *fn*). This appears to suggest that the development of tip vortex cavitation is affected by the non-uniform flow field through the guide vanes.

Air was injected at a constant $\sigma^* = 0.946$. Vibration levels were reduced 50 % for an air flow rate of $Q_a = 0.4$ ‰ at the expense of an efficiency drop of less than 1 %. Air flow rates greater than 0.8 ‰ do not induce any further reduction of the level of vibration while causing the efficiency to decay.

Further tests are to be performed on a prototype, aiming at determining the optimum air flow rate, size and distribution of the injectors.

6. Acknowledgement

The authors would like to thanks to Oscar Héctor Capezio and the technical team of the Yacyreta power station for their contribution. Special thanks to the technical team of the test rig, Martín Zagaglia, Martín Rodríguez, and Leonardo Díaz.

7. References

[1] Franc, JP, Avellan F, Kueny JL, 1995: La cavitation: mécanismes physiques et aspects industriels. Grenoble: Presses universitaires de Grenoble PUG.

[2] Rus T, Dular M, Sirok B, Hocevar M and Kern I, 2007: An investigation of the relationship between acoustic emission, vibration, noise and cavitation structures on a Kaplan turbine. ASME Transactions Vol 129.

[3] Ruchonnet N, Nicolet C, Avellan F 2006:Hydroacoustic Modeling of Rotor Stator Interaction in Francis Pump-Turbine. IAHR Int. Meeting of WG on Cavitation and Dynamic Problems in Hydraulic Machinery and Systems. Barcelona, Spain.

[4] Rivetti A, Lucino C, Liscia S, Muguerza D, Avellan F 2012: Pressure Pulsation in Kaplan Turbines: Prototype – CFD Comparison. 26th IAHR Symposium on Hydraulic Machinery and Systems. Beijing, China.

[5] Rivetti A, Lucino C, Liscia S, 2013: Guide Vane Influence on Pressure Fluctuation at the Discharge Ring in a Kaplan Turbine: Experimental Assessment. I IAHR Latin American Hydro Power and Systems Meeting , Campinas, Brazil.

[6] Nennemann B and Vu T C, 2007: Kaplan turbine blade and discharge ring cavitation prediction using unsteady CFD. 2nd IAHR international meeting of the workgroup on cavitation and dynamic problems in hydraulic machinery and systems. Timisoara, Romania.

[7] IEC standars. Hydraulic turbines, starages pumps and pumps-turbines-model acceptance tests; IEC60193-1999.